Available online at www.sciencedirect.com
ScienceDirect
Proceedings of the Combustion Institute 38 (2021) 5109–5117
Proceedings of the Combustion Institute
www.elsevier.com/locate/proci

Flame spread behavior characterization of discrete fuel array under a forced flow

Giovanni Di Cristina [a], Nicholas S. Skowronski [b], Albert Simeoni [c], Ali S. Rangwala [c], Seong-kyun Im [a,d,*]

[a] Department of Aerospace and Mechanical Engineering, University of Notre Dame, Notre Dame, IN, United States
[b] USDA Forest Service, Northern Research Station, Morgantown, WV, United States
[c] Department of Fire Protection Engineering, Worcester Polytechnic Institute, Worcester, MA, United States
[d] Department of Mechanical Engineering, Korea University, Seoul, Republic of Korea

Received 8 November 2019; accepted 29 May 2020
Available online 28 July 2020

Abstract

The forced flow driven flame spread behavior along an array of discrete wooden fuel elements was experimentally investigated, which could be an important step to understanding the flow-flame interactions that govern fire spread. Fuel arrays with five different spacings (0.75, 0.875. 1.00, 1.125, and 1.25 cm) were subject to flow speeds ranging from 2.2 to 4.3 m/s at approximately 0.2 m/s intervals. For spacing-flow speed conditions tested in the current study, the flame spread behavior was categorized into three different regimes, continuous, discrete, and quenching, and the regimes were presented in a flammability map. Visual analysis of top and side view video data were used to describe the changing flame behavior and increasing discretization of the overall flame structure as the flow speed increases. An analysis of the fluid mechanics and heat transfer conditions revealed a correlation between the Stanton number (*St*), the Damkohler number (*Da*), and the onset of flame instabilities and quenching.

Keywords: Flame spread; Quenching; Wood combustion; Flow-flame interaction; Wind-driven fire

1. Introduction

Small-sized wooden sticks or dowels have been used to represent the initiation and early buildup of a forest fire, where the first vegetation involving initial ignition processes are the small leaves, pine needles, and branches. Early fire spread research by Fons [1] and Emmons [2,3] modeled the consecutive ignitions of fuel elements in arrays and simple fuel beds to represent non-homogeneous forest fuel beds. Since then, researchers have used

* Corresponding author at: Professor Seong-kyun Im, Department of Mechanical Engineering, Korea University, 319 Innovation Hall, 145 Anam-ro Seongbuk-gu, Seoul 02841, Republic of Korea.
E-mail addresses: sim3@korea.ac.kr, sim@nd.edu (S.-k. Im).

https://doi.org/10.1016/j.proci.2020.05.035
1540-7489

arrays or fuel beds of wooden sticks, paper strips, cardboard or other simple fuels to simplify the study of complex fire scenarios [1,3–12].

Vogel and Williams [4] examined the spread along square dowels mounted on a plate at different spacing conditions and found that the spread can be accurately approximated using a 1-dimensional conduction model. Prahl and Tien [5] expanded on the work of Vogel and Williams [4] by subjecting a similar setup to convective flows of up to 0.9 m/s. While Prahl and Tien [5] predicted the spread rate of their wind-driven experiments, they could not accurately predict the onset of no propagation for the higher wind speed conditions. Beer [11] developed a purely geometric model for fire spread of arrays subject to flow or slope by using similar assumptions from Vogel and Williams [4]. In Beer's model, the flow (or slope) only serves to tilt the flame but does not account for other effects of the flow, such as quenching from high wind speeds.

Although the previous works have demonstrated predictions and modeling of fire spread behaviors under a flow with a relatively low speed (below 1.5 m/s), studies for the fire spread behaviors were relatively rare for the flow conditions above 1.5 m/s, where the buoyancy effects on the flame are still comparable to the effects of momentum from the imposed flow. Furthermore, it has been reported that fire spread around the 2.5 mm diameter scale becomes unsteady and highly variable at relatively high flow speeds (around 3 m/s) [13]. The propagation and flame behavior changes at extinction conditions in fuel arrays have not been studied previously. Studies for unsteady flames near extinction have been conducted for single cylinders [14] and tandem spheres [15] but not for cylinder arrays. Extensive studies on fluid mechanics of single cylinders, tandem cylinders [16–18], and cylinder arrays and banks [19,20] inform how the convective flow may interact with the cylinders. Such interactions alter the convective heat transfer depending on the separation distance and flow speed. For a reacting flow, the flame-flow coupling can cause unique flame dynamics and spread behaviors. Finney et al. [21] suggested that unsteady flame convection is strongly dictated by buoyant and inertial interaction, and the findings could contribute to advancing physics-based modeling.

The current study seeks to provide further discussion on the flame-flow coupling, arguing that the common assumptions of continuous increase in flame contact or convective heat transfer with an increasing freestream flow speed should be adjusted if the flow and fuel setting lead to discretized flame behavior. The flame-spread behavior of discrete solid fuels was characterized at flow speeds above 2 m/s for multiple spacing conditions. The systematic classification and corresponding analysis of the flow conditions are used to generate a flammability map for flame spread on discrete fuels under forced flow. For example, in an array of dowels, the ignition of the dowel at position *n* will depend on the flame heat transfer of upstream dowels at positions (*n-1, n-2*, etc.) that further depend on the upward and downward spread rates on each dowel based on the flow velocity, separation distance, and material properties. The problem is further complicated by the flame-flow instabilities triggered at certain flow speed-array spacing conditions. The ability to predict the onset of such flame instabilities due to convective conditions could be the first step in extending the accuracy of flame spread models.

2. Experimental setup

Wooden dowels with a diameter (d) of 3.2 mm and a length of 14 cm were arranged into in-line arrays. Mounting plates with drilled holes at the desired spacings were manufactured, and the dowels were press-fit to the holes. The mounting plate was then placed in a small wind tunnel with a test section that has a cross-sectional area of 15.25 cm by 15.24 cm and length of 81.28 cm, as schematically illustrated in Fig. 1a. Flow conditioning screens were utilized to achieve a uniform flow profile across the height of the wind tunnel and minimize fluctuations to less than 5% of the mean flow. A pilot ignition using a small cotton wick soaked in 0.1 ml of dodecane initiated the fire 1 cm ahead of the first dowel as shown in Fig. 1b. The pilot was ignited after turning the flow on in order to avoid flow unsteadiness from the fan startup. Because the pilot ignition could affect the flame propagation, the ignition method was kept consistent for all experiments.

Flame propagation was measured with two cameras, a GoPro camera facing the dowel array and a Sony DSCIII facing downward. The side camera visualized the flame propagation behavior while the downward-facing camera captured the flame wake. The flame propagation behavior was studied for 5 spacings ($s = 0.75$, 0.875, 1.00, 1.125, and 1.25 cm) under freestream flows of 2.2 to 4.3 m/s at approximately 0.2 m/s increments. The smallest spacing (0.75 cm) was selected based on the flame size without wind, at which the flame barely touches the next dowel. The buoyancy currents exit the test section before they impact the ceiling with the flow speeds chosen in the current study, minimizing ceiling effects. For each spacing-velocity combination, the experiments were repeated 3 times. In addition to the flame spread experiments, a hot-wire anemometer was utilized to measure the mean flow speed and turbulent intensity behind dowel 5 of the array in cold flows. Measurements were taken approximately 6 cm above the base of the tunnel at the centerline of the cylinder longitudinal axis. Flow data was collected at a half-spacing distance away from dowel 5 at all spacing conditions.

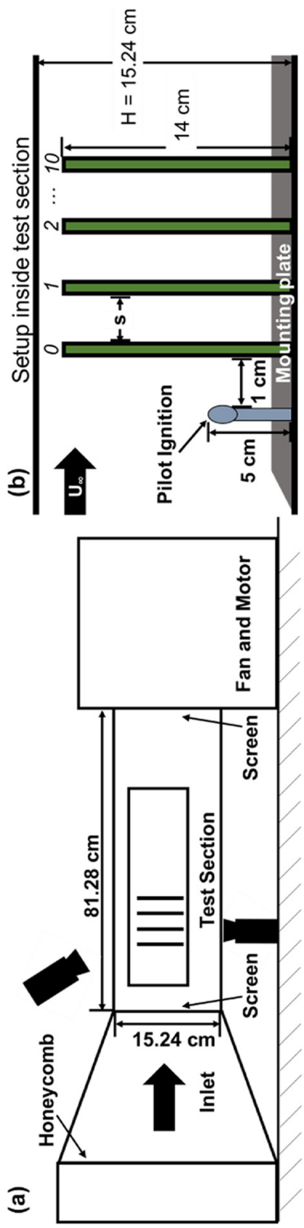

Fig. 1. (a) Schematic of wind tunnel and (b) dowel array setup inside the wind tunnel test section.

3. Results

3.1. Flame propagation behavior characterization

From the time the pilot is ignited, the very first dowel is in contact with the flame. The first dowel will then begin to char and eventually ignite. The ignition kernel is observed in the wake of the dowel. Subsequent ignition of downstream dowels then depends on contact from the upstream ignited fuel elements. As the flame propagates through the array and more dowels are burning simultaneously, the flame spread accelerates and reaches a steady-state around the 4th dowel position. By the time the last dowel position ignites, upstream dowel positions in the early stages of spread have been consumed and are no longer flaming.

At each spacing-velocity test condition, the flame propagation behavior was classified into three regimes; continuous flame spread (I), discrete flame spread (II), and no propagation (III). Fig. 2 depicts the key differences of each regime classification for various flow speeds at a fixed spacing of 1 cm. It should be noted that dowel bending does occur, affecting the dowel spacing. However, dowel bending typically occurs at the later stages of flame propagation. When bending is observed, the flame has already reached a few dowels downstream, and it would have a minimal effect on the quantities reported.

In the continuous regime (I), each flaming dowel contributes to an overall flame that encompasses the array. The largest flame areas are seen in this regime, and typical flame angles are in the range of 25° to 30°, lower than Prahl and Tien [5] who observed 40° to 70° As the wind speed increases, the large flame brush breaks down into discrete flames (II) attached to each dowel, and the discrete flames do not combine into one flame structure. The flame length is also reduced. The increased flow momentum causes the flame angle to decrease from approximately 25° to 10°. As evidenced by the shorter char height (b), the overall flame contact area is also reduced compared with the continuous regime (I). For regime II, the flame length around each dowel shortens to an extent, and a noticeable gap (Δy) is observed between the flame and the adjacent dowel. With further increase in the flow speed, the flame length is further reduced, and Δy increases. The increase in Δy results in reduced heat transfer from one dowel to the next which reduces the global flame spread rate. The flame also flickers laterally. The combination of the reduced flame length, high flickering, and reduced flame area leads to an arrest of flame propagation past the first few dowels after the pilot and eventually quenching. The velocity-spacing condition leading to quenching is classified as the quenching regime (III).

Each flow-spacing condition was categorized into the corresponding regime based on the flame

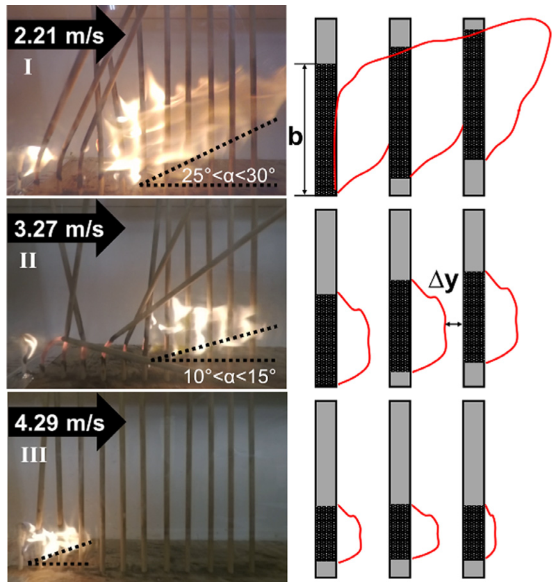

Fig. 2. Images and sketches of the continuous (I), discrete (II), and quenching (III) flame spread behaviors observed in a 1 cm spaced array.

behavior visualized by the side-view camera, and the results are shown in Fig. 3. Experimental results from Vogel and Williams [4] and Prahl and Tien [5] are also plotted. In Fig. 3, each regime is delineated by hand-drawn lines to qualitatively describe the trend of the boundary change for various normalized spacing (s/d) and Reynolds number (*Re*) based on the dowel diameter (d). It should be noted that transition conditions (solid gray circle) between the continuous and discrete flame spread regimes are also shown in Fig. 3, at which both continuous and discrete flame spreads were observed within 3 repetitions of the experiments.

When the flow speed and spacing are low, the flame spread is in the continuous regime (I), where the flow tilts the flame, thereby touching the next fuel elements. When the spacing is comparatively small ($s/d < 4.15$), continuous flame spread persists even at high flow speeds (greater than 3 m/s) known to cause instabilities in flame spread at larger spacings [13,22]. Once the spacing is increased greater than approximately $s/d = 4.15$ (1 cm spacing), continuous flame spread is difficult to sustain above $Re = 500$ (2.5 m/s). Further increase in the flow speed or spacing causes the flame on each element to shrink, such that it no longer touches the adjacent dowel, and discrete flame behavior (regime II) is observed. Note that the discrete regime can also occur at low flow speeds with larger spacings. Thus, it is reasonable to presume that at a large enough spacing the only possible sustained flame spread would be discrete. Likewise, at a small enough spacing only continuous flame spread would be observed for all flow speeds below the blow-off limit. When the flow speed or spacing becomes sufficiently large, sustained propagation in the array becomes impossible (regime III).

The current experimental data combined with data from the literature suggests that the threshold boundary for quenching seems to take on a hyperbolic shape, with the vertex approximately at s/d ~7.5 and between 1.5 and 2 m/s. Within regime III for flow slower than 2 m/s, the quenching is because of spacing being too large for the upstream flame to overcome and ignite the next fuel element, which is more akin to extinction. For flow speeds above 2 m/s, the flow introduces flame instabilities and highly fragmented flames, and here the propagation cessation is more akin to blow-off. It would be natural to assume that the discrete propagation boundary, similar to the quenching boundary, would also follow a hyperbolic trend (dashed-line) although further investigation is needed to delineate the boundary.

3.2. Flame structure

Each flame propagation regime has a distinct flame structure, and both the flame shape and propagation are strongly affected by the flow and spacing. In order to analyze the effects of increasing flow on the flame shape, images of the side and top view are compared. Fig. 4 shows schematics of the flames and flame images of the side and top views at the time of ignition of dowel 5 for a constant spacing (1.00 cm) and 4 flow conditions, 2.42, 2.82, 3.27, and 3.63 m/s ($Re = 486$, 570, 660, and 740).

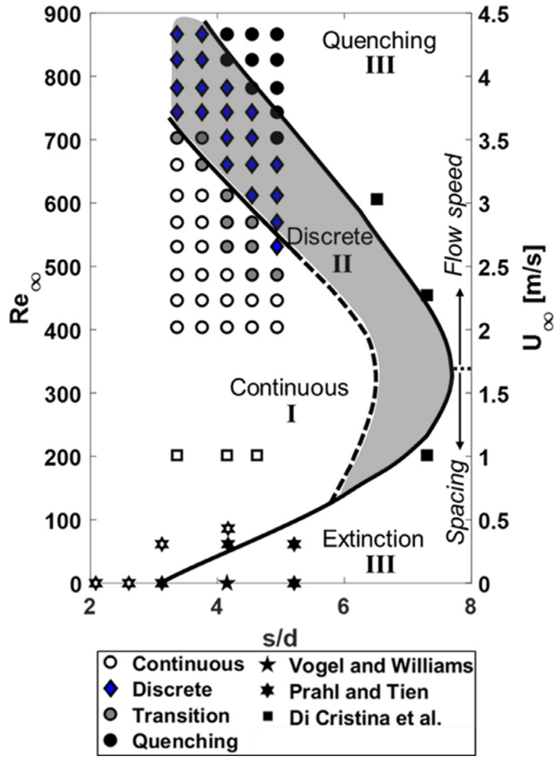

Fig. 3. Flame spread regime map showing Continuous (I), Discrete (II), and Quenching/Extinction (III) regimes as a function of flow and spacing of discrete fuel array.

The schematics in Fig. 4 illustrate the behavioral trends of the flame from dowel 4 as it interacts with, and ignites, dowel 5 for increasing flow speeds. At flow speeds of 2.42 and 2.82 m/s, within the continuous flame spread regime (I), the flame attaches on the leading edge of the upstream cylinder (dowel 4 in Fig. 4) forming a flame envelope that extends past the downstream cylinder (dowel 5) through the wake region and impinges on the leading edge of the downstream cylinder. As the flow speed increases from 2.42 to 2.82 m/s, the wake width (W) increases while the length (L) decreases, similarly observed in other forced convection studies [5,23]. Additionally, the standoff distance in front of the upstream dowel reduces, and the flame envelope begins to recede. For the discrete flame spread (regime II, 3.27 m/s), the wake is widened significantly. Also, the length of flame is further decreased, barely passing the downstream cylinder, and the standoff distance reaches zero attaching onto the leading edge of the cylinder. The length of the flame fluctuates, but the wake flame remains in the inter-cylinder region rather than going past the downstream cylinder. As the velocity continues to increase, the length continues to decrease until it is only sustained in the inter-cylinder region. The length will keep decreasing correspondingly with the increasing flow speed. The most fragmented flames are present at the flow speeds just below the quenching (regime III) threshold, the flame envelope previously observed transitions into a wake flame as seen in the far right images under a flow of 3.68 m/s in Fig 4. The changes in wake width and length are further described in Fig. 5 which shows the width to length ratio of the wake flame (W/L) around dowel 4 at the time when dowel 5 is igniting. It should be noted that the effect of spacing on the flame shape does not seem to be linear. However, in general, W/L increases and reaches an asymptotic value as the wind speed increases. A high W/L is indicative of highly discretized flame behavior.

For fire spread in the continuous flame regime (I), although the cylinder leading edge shows some charring, ignition occurs at the trailing edge of the cylinder where the local flow speed is slowest, resulting in the maximum residence time. In contrast, for regime II, the ignition typically occurs near the two flow separation points of the dowel cylinder, as shown in Fig. 4. At this location, the flow is at an intermediate speed between the faster freestream and slower wake region, and the surface temperature would be higher as the upstream flame shortens. Similar ignition location

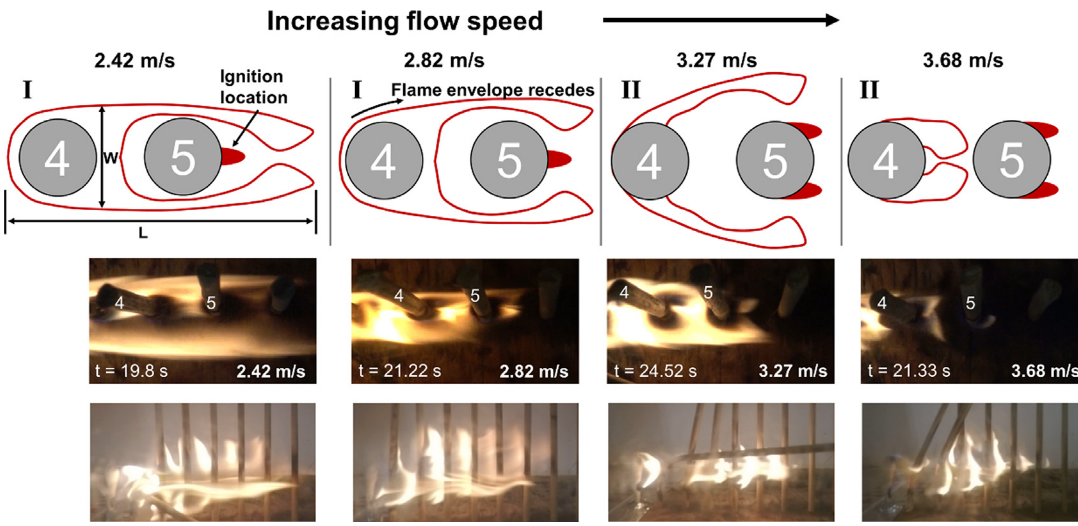

Fig. 4. Schematics (top row) of flame (hollow red line) and ignition location (solid red) and top (middle row) and side (bottom row) view images of dowel 5 ignition for 1 cm spacing at 4 flow speeds Timestamps are relative to pilot ignition.

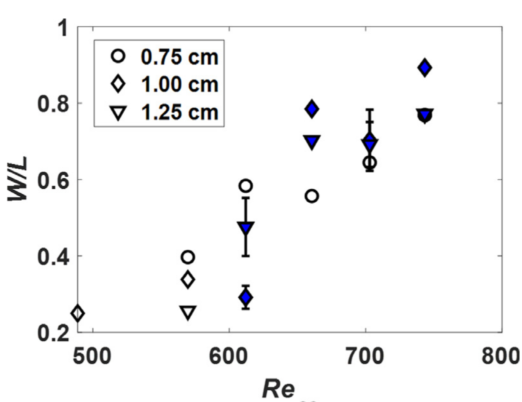

Fig. 5. Wake flame width to length ratio *(W/L)* for a range of flow speeds and array spacings. The filled markers represent discrete flame behavior at those conditions.

behavior has been observed in droplet combustion by Fernandez-Pello and Law [23].

It is important to note that the regime classification was based on the side view flame images. The drastic change in flame shape between 2.82 and 3.27 m/s is evident from Fig. 4. The discrete flame cases have little to no cohesion in the overall flame, with each dowel burning independently, along with a significant decrease in the flame contact area. The decrease in the flame contact area is also in contradiction with some fire propagation models [5,11] that are based on the assumption that faster flow speeds increase the contact area. Thus, there may be a limit to the applicability of the assumption that faster flow leads to greater flame contact. Although not shown, at a constant flow speed, increasing the spacing has the same effect on the overall flame shape as increasing the flow speed for a fixed spacing.

3.3. Regime boundary prediction

Ignition of a solid fuel requires sufficient heating to be pyrolyzed such that the pyrolyzates mix with an oxidizer to create a flammable mixture. Then, the mixture can be ignited. Because the pyrolyzing process is the slowest process, the pyrolysis time scale could be regarded as the time scale for ignition. In the current study, by considering the size of the flame and flow settings [4,7,13], it is assumed that convection is the dominant source of heat transfer and radiative heat transfer is much smaller than the convective heat transfer. For a forced flow environment, enough heat must penetrate the boundary layer along the surface to increase temperature of the solid fuel, which also needs accounting for ignition prediction. The heat transfer through a boundary layer is typically quantified by using the Nusselt number (Nu). The Nusselt number (and correspondingly the heat transfer coefficient) was calculated by using an empirical correlation for cylinder banks in crossflow [17] shown as Eq. (1),

$$Nu = 1.367\left[0.25 + e^{(-0.55(s/d))}\right](s/d)^{0.212} Re^{1/2} Pr^{1/3} = \frac{hd}{k}, \tag{1}$$

where, Re, Pr, h, and k are Reynolds number, Prandtl number, convective heat transfer coefficient, and thermal conductivity, respectively. Pr was assumed to be 0.7, and k of 2.624×10^{-5} kW/mK was used similar to other studies with the same fuel [4,7]. The values of h calculated from Eq. (1) were used to estimate the boundary layer length (δ_{BL}) by following the method outlined in Quintiere [24], as shown in Eq. (2). In this study, the local mean flow velocity behind dowel 5, as measured with a hot-wire anemometer, was utilized instead of the freestream velocity for calculations of the boundary layer. The boundary layer length is then used to approximate the mixing time (t_{mix}) from Eq. (3). The mass diffusivity (D) was assumed to be the value of CO at 600 K since CO would be the dominant gas species in combustion products, and 600 K is typical fuel pyrolysis surface temperature [24].

$$h \approx \frac{k}{\delta_{BL}}, \tag{2}$$

$$t_{mix} \approx \frac{\delta_{BL}^2}{D} \tag{3}$$

Although the Nusselt number (more specifically h) gives an idea of how much convective heat transfer is delivered to the dowel surface, it cannot account for convective cooling at higher flow speeds. Therefore, the Stanton number (St) is utilized, which can be thought of as a modified Nusselt number, the ratio of convective heat transfer to the heat capacity of the fluid shown as Eq. (4),

$$St = \frac{Nu}{RePr} = \frac{h}{\rho U_\infty c_p} = \frac{h/U_\infty}{\rho c_p}, \tag{4}$$

where ρ and c_p are density and specific heat of the gas, respectively. Therefore, when the flow velocity increase, the amount of heat that the fluid can absorb instead of transferring to the solid fuel also increases. Note that the Stanton number (St) was identified by Quintiere [24] as a pertinent dimensionless quantity and can be defined as $St = h/\rho c_p (gl)^{1/2}$ when buoyancy is dominant.

Pyrolysis alone does not dictate the ignition of the solid fuel and flame propagation along the array. Therefore, using St alone may not be sufficient for prediction. As seen in Figs. 2–4, quenching occurs although the pilot flame still provides the necessary heat to pyrolyze. Therefore, other transport phenomena could also play a role in ignition and flame propagation. The mass transport of the flammable mixture with respect to chemical reactions also affects ignition and flame propagation. Therefore, the Damkohler number (Da) is used to predict the flame propagation boundary in addition to St. In the current study, the mixing time scale is used to represent the mass transport time scale. Eqs. (5) and (6) presents the Damkohler number definition and chemical time scale, with Eq. (3) used as the mixing time scale.

$$Da = \frac{t_{mix}}{t_{chem}}, \tag{5}$$

$$t_{chem} = \frac{0.623kT}{\alpha[E/(RT)]A\Delta h_c e^{-E/(RT)}}. \tag{6}$$

Here, α (1.25×10^{-7} m^2/s), Δh_c (16.3 kJ/g), T (1600 K), E, R ($E/RT = 16$), A (10^{13} g/m^{3}s) are the thermal diffusivity, heat of combustion, flame temperature, activation energy, gas constant, pre-exponential Arrhenius constant, respectively. For the chemical time, estimates for the constants were taken from literature for wood [7,24]. In the current study, the chemical time is constant. Thus, Da is changed due to the changes in the mixing time. Da is multiplied by d/s to account for the effects of spacing on ignition and flame propagation. Fig. 6 shows a plot of the Stanton number (St) vs. scaled Damkohler number ($Da(d/s)$) similar to a functional St – Da relationship used by Quintiere in describing flame propagation on a solid block. A full range from St = 0 to 0.1, is shown in Fig. 6a, with a zoomed-in view of the current experiments shown in Fig. 6b [24].

The flow-spacing conditions used in this study collapse reasonably onto a fitted logarithmic regression line (Fig. 6a). $Da(d/s)$ decreases as either flow speed increases or spacing increases. Thus, quenching could occur at low enough $Da(d/s)$ values. It seems that $Da(d/s)$ approaches an asymptote as St increases. At lower wind speeds, mixing would generally be weak and not sensitive to the flow speed. By manually inspecting flame images, it was observed that there is less fluctuation of the flame, which indicated less mixing as flow speed decreases. Since flow speed decreases as St increases, the mixing or $Da(d/s)$ becomes less sensitive to the flow speed. Also, when the spacing becomes small enough, the discrete solid fuel array would behave like a continuous fuel. Thus, the flame propagation behavior also becomes less sensitive to the flow as the spacing decreases, especially when St is higher.

The boundaries of the onset of both discrete flames (regime II) and flame spread quenching (regime III) are reasonably well captured by St (Fig. 6b). A lower St corresponds to faster flow speeds and ultimately flame quenching due to insufficient heat delivered to the next unignited dowel. For the current experiments, St below 0.028 and over 0.033 correspond to the quenching regime (III) and the continuous regime (I), respectively. For a comparison, numerical data of a single PMMA cylinder in crossflow by Yang and Tien [14] is shown alongside the experimental data. The flame blowoff conditions found by Yang and Tien [14] agree with the St threshold for quenching of the current experiments. As St increases, between approximately St values of 0.028 and 0.033, the convective cooling effects decrease such that propagation is sustained but in a discrete regime (II). When St is greater than 0.033, the flow is slow enough that flame propagation is in the continuous

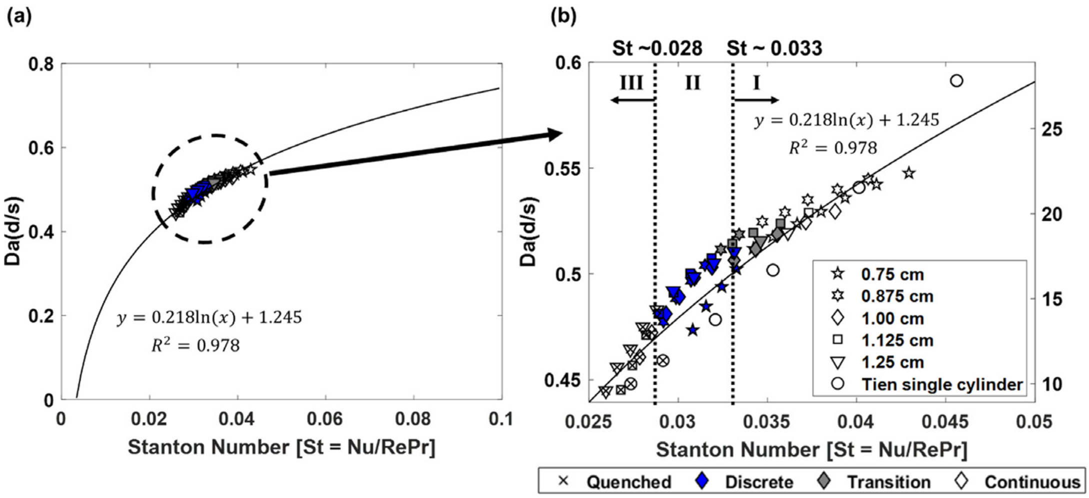

Fig. 6. *St* vs. *Da(d/s)* plot comparing the experimental data to a logarithmic regression (a) and zoomed-in plot (b) showing flow-spacing conditions in detail of the current study and from the single cylinder Yang and Tien study that uses the right y-axis [14].

regime (I). Further experiments are needed to validate the applicability of the shown regression at both larger and smaller *St* values.

4. Conclusion

Three fire spread behavior regimes were identified for a fuel array under a range of flow and element spacing conditions. These regimes correspond to how each individual flaming dowel contributes to the overall flame spread, whether the flame is continuous (regime I), discretized (regime II) about each dowel, or propagation is unsustained (regime III). The flame shapes within the propagating regimes showed how initially the upstream flame extends past the downstream cylinder. As the flow speed is increased, the flame begins to encroach and lie in the inter-cylinder region. The ignition location also shifts from directly in the wake where the mixing time is longest due to slower flow speed to the flow separation points along the cylinder where the surface temperature is higher. The side view showed how the overall flame shape changes and the contact area is reduced with increasing flow speed. The analysis of the time scales, fluid dynamics, and heat transfer revealed a correlation between the Stanton number and Damkohler number. The correlation exhibits a threshold that corresponds to the onset of the three flame spread regimes. Further work is required to fill in the gaps and solidify the assumed boundaries of the flame spread map (Fig. 3). Additionally, the scaling of the flow regimes for other dowel diameters and orientations needs to be explored. However, this study suggests that assumptions of continuous increase in flame contact or convective heat transfer with increasing free stream flow should be adjusted if the flow and fuel setting lead to a discretized flame behavior.

Declaration of Competing Interest

None.

Acknowledgments

This work was supported by U.S. DOD/EPA/DOE Strategic Environmental Research Development Program (SERDP, Project Number: RC-2641). Seong-kyun Im was supported by Korea University research grants.

References

[1] W.L. Fons, *J. Agric. Res.* 72 (1946) 93–121. https://doi.org/10.1016/j.jns.2003.09.014.
[2] H.W. Emmons, *Fire Res. Abstr. Rev.* 5 (1963) 163–175.
[3] H.W. Emmons, T. Shen, *Symp. Int. Combust.* 13 (1971) 917–926. https://doi.org/10.1016/S0082-0784(71)80092-9.
[4] M. Vogel, F.A. Williams, *Combust. Sci. Technol.* 1 (1970) 429–436. https://doi.org/10.1080/00102206908952223.
[5] J.M. Prahl, J.S. Tien, *Combust. Sci. Technol.* 7 (1973) 271–282. https://doi.org/10.1080/00102207308952367.
[6] M.F. Wolff, G.F. Carrier, F.E. Fendell, *Combust. Sci. Technol.* 77 (1991) 261–289. https://doi.org/10.1080/00102209108951731.
[7] M.J. Gollner, Y. Xie, M. Lee, Y. Nakamura, A.S. Rangwala, *Combust. Sci. Technol.* 184 (2012)

585–607. https://doi.org/10.1080/00102202.2011.652787.

[8] L. Jiang, Z. Zhao, W. Tang, C. Miller, J.H. Sun, M.J. Gollner, *Proc. Combust. Inst.* 000 (2018) 1–8. https://doi.org/10.1016/j.proci.2018.09.008.

[9] C.H. Miller, M.J. Gollner, *Fire Saf. J.* 77 (2015) 36–45. https://doi.org/10.1016/j.firesaf.2015.07.003.

[10] R.O. Weber, *Math. Comput. Model.* 13 (1990) 95–102. https://doi.org/10.1016/0895-7177(90)90103-T.

[11] T. Beer, *Int. J. Wildland Fire.* 5 (1995) 43–49. https://doi.org/10.1071/WF9950043.

[12] D. Weise, G. Biging, *Fire Saf. Sci.* 4 (1994) 1041–1051. https://doi.org/10.3801/IAFSS.FSS.4-1041.

[13] M.F. Wolff, G.F. Carrier, F.E. Fendell, *Combust. Sci. Technol.* 77 (1991) 261–289. https://doi.org/10.1080/00102209108951731.

[14] C.T. Yang, J.S. T'ien, *J. Heat Transf.* 120 (1998) 1055–1063. https://doi.org/10.1115/1.2825890.

[15] V. Raghavan, V. Babu, T. Sundararajan, *Combust. Theory Model.* 13 (2009) 461–485. https://doi.org/10.1080/13647830902822198.

[16] B.S. Carmo, J.R. Meneghini, S.J. Sherwin, *Phys. Fluids.* 22 (2010) 1–7. https://doi.org/10.1063/1.3420111.

[17] B.S. Carmo, J.R. Meneghini, S.J. Sherwin, *J. Fluid Mech.* 644 (2010) 395. https://doi.org/10.1017/S0022112009992473.

[18] D. Sumner, *J. Fluids Struct.* 26 (2010) 849–899. https://doi.org/10.1016/j.jfluidstructs.2010.07.001.

[19] Bejan, *Trans. ASME J. Heat Transf.* 117 (1995) 767–770. https://doi.org/10.4103/0019-557X.115003.

[20] Y. Bao, Q. Wu, D. Zhou, *Comput. Fluids.* 55 (2012) 118–131. https://doi.org/10.1016/j.compfluid.2011.11.011.

[21] M.A. Finney, J.D. Cohen, J.M. Forthofer, S.S. McAllister, M.J. Gollner, D.J. Gorham, K. Saito, N.K. Akafuah, B.A. Adam, J.D. English, *Proc. Natl. Acad. Sci.* 112 (2015) 9833–9838. https://doi.org/10.1073/pnas.1504498112.

[22] F.R. Steward, L.J. Wuest, R.T. Waibel, *Heat Transf. Div. Pap.* (1977).

[23] A.C. Fernandez-Pello, C.K. Law, *Symp. Int. Combust.* (1982) 1037–1044.

[24] J.G. Quintiere, *Fundamentals of Fire Phenomena*, John Wiley & Sons Ltd, 2006 https://doi.org/10.1002/0470091150.